

# ANALYSIS OF THE HEADWATER BASINS' MORPHOLOGY BY HIGH-RESOLUTION LIDAR-DERIVED DTM

P. Tarolli<sup>a,\*</sup>, G. Dalla Fontana<sup>a</sup>

<sup>a</sup>Dept. of Land and Agroforest Environments, University of Padova, viale dell'Università 16, 35020 Legnaro, PD, Italy  
- (paolo.tarolli, giancarlo.dallafontana)@unipd.it

**KEY WORDS:** LiDAR, DTM, headwater catchment, river morphology, landslides.

## ABSTRACT:

High resolution topographic data have the potential to differentiate the main morphological features of a landscape. For the purpose of this study the Digital Terrain Models (DTMs) ranging between 1m and 20m (cell size) were derived from the last pulse LiDAR data by filtering the vegetation points. We tested the effects of different resolutions in the analysis of river morphology, and potential slope stability. The study was conducted in two headwater catchments located in the eastern Italian Alps where a high-quality set of LiDAR data was available. The results indicated for higher DTM resolutions an improved effectiveness in the recognition of river morphology. Otherwise the progressive finer DTM resolution does not necessarily improve the interpretation of slope stability processes especially if landslides occur at a spatial scale significantly greater than cell size.

## 1. INTRODUCTION

The accuracy of procedures relying on topographically-based analysis of catchment processes strongly depends on the availability and quality of the topographic data. With respect to the quality, the accuracy of bare ground elevation points and the method used to interpolate the Digital Terrain Model (DTM) can affect the results of some derived applications. New survey techniques have been introduced in the last few years. One of these is the use of airborne laser altimetry (Akermann, 1999; Kraus&Pfeifer, 2001; Briese, 2004). This technology, named LiDAR (Light Detection And Ranging), provides high-quality digital terrain data than previously available. The application of airborne laser altimetry technology to physically-based process modeling or any other topographically derived analysis has the potential to enhance the model performance, to improve the quality of the results and to benefit the land management. Anyway, the degree to which the resolution of LiDAR-derived DTM affects the representation of the land surface, the spatial variability of physical catchment processes has not yet been examined systematically. High resolution DTMs may help to detect landslide areas by the analysis of the surface roughness (McKean and Roering, 2004), and allows the characterization and differentiation of landslide morphology and activity (Glenn et al., 2006). Otherwise Tarolli and Tarboton (2006) developed a study in which, while discussing a new method for mapping the most likely landslide initiation points, they noticed that a high-resolution LiDAR-derived DTM may affect the performance of a terrain stability model. In fact, there may be some limitations to the improvement of landslide modeling when using topographic data at a very fine resolution. At very fine resolution, DTM-derived slopes may no longer be representative of the reference critical slope in the infinite-slope stability model (Tarolli and Tarboton 2006). The aim of this work was to analyze the effects of LiDAR-derived DTM resolution on some related applications. We tested the effects of LiDAR-derived DTMs with different grid cell sizes ranging from 1m to 20m. In the analysis, we took into consideration the

detection of river morphology and the potential slope stability mapping.

## 2. STUDY AREA

The study area are two small alpine basins (Rio Cordon and the head water catchment of Miozza basin), located respectively in the Dolomite and Carnia, two alpine regions in the north-east of Italy (Figure 1).

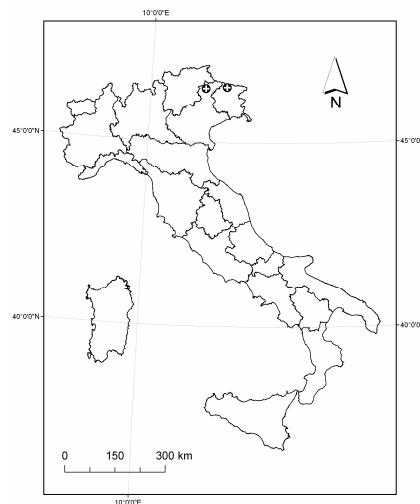


Figure 1. Location map of study areas

### 2.1 Rio Cordon basin

The basin (Figure 2) covers 5 km<sup>2</sup>. Elevations range between 1763 and 2748 m a.s.l., with an average value of 2200 m a.s.l. The basin is highly dissected with hillslope lengths on the order of 40–60 m. Average slope is 27°, slopes of 30–40° are

\* Corresponding author.

common, and there is a substantial number of slopes that locally exceed  $45^\circ$ . The area presents a mean annual rainfall of about 1100 mm. Precipitation occurs mainly as snowfall from November to April. In summer storm events are usually intervalled by long dry spell. Vegetation cover consists mainly of herbaceous associations (61%); shrubs are rather widespread (18%), while forest stands made up by spruce and larch are found only in the lower part of the watershed and occupy 7% of the total area.

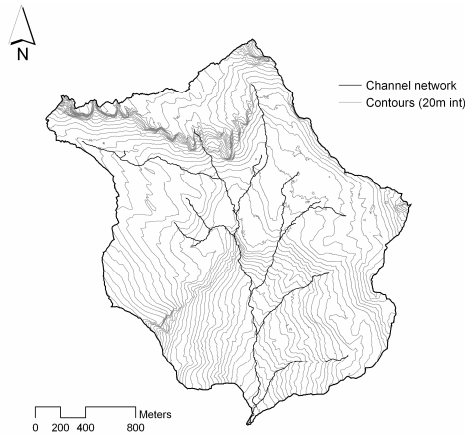


Figure 2. Rio Cordon basin

### 2.2 Head water catchment of Miozza basin

The area (Figure 3) covers  $4.4 \text{ km}^2$ . The elevation ranges from 834 to 2075 m a.s.l., with an average value of 1530 m a.s.l. The slope angle has an average value of  $35^\circ$ , reaching maximum values of  $73^\circ$ . The area presents a mean annual rainfall of about 2200 mm. Precipitation occurs mainly as snowfall from November to April. Recorded annual precipitation ranges from 1300 to 2500 mm. In summer, flash floods with heavy solid transport and debris flows are common. Vegetation covers 91% of the area and consists of forest stands (64%), shrubs (19%) and mountain grassland (17%); the remaining 9% of the area is unvegetated landslide scars (8%) and bedrock outcrops (1%). The geomorphologic setting of the basin is typical of the eastern alpine region, with deeply incised valleys. Soil thickness varies between 0.2 m and 0.5 m on topographic spurs and depths of up to 1.5 m in topographic hollows. There is no human activity within the basin.

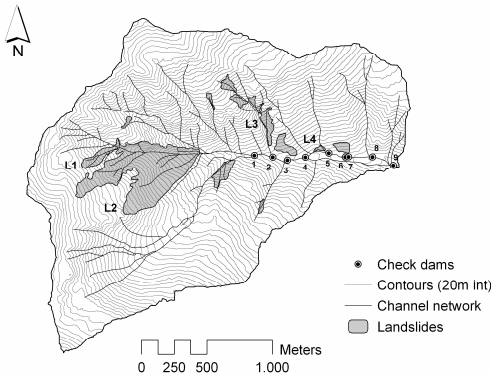


Figure 3. Headwater catchment of Miozza basin

Within the study area, landslides have been mapped and the erosion zone and shallow landslide scars amounts to  $0.35 \text{ km}^2$ , i.e. about 8% of the total catchment area. In the Figure 4 is showed the triggering area of landslide L1 (Figure 3)



Figure 4. Landslide complex at the head of the basin (detail of the field site L1 reported in the Figure 3).

Aerial photographs having a 0.5 m-resolution and field mapping were used to develop a detailed inventory of sediment sources, erosion and landslide scars. The mapped landslides covered the entire landslide scar, including the runout zone, and were not limited to the areas where the landslides started. The most recent aerial photographs were used to identify recent landslides which did not appear in earlier surveys. The landslides identified in the aerial photographs were checked in the field. The average slope of the landslide scar area is  $41^\circ$ . Most of these areas, in particular the largest single landslide section ( $0.22 \text{ km}^2$ ), are located at the head of the basin and result from the aggregation of few shallow landslides. Some of the landslides occurred at the bedrock interface while others occurred in the soil upper part ( $\sim 0.5 \text{ m}$  deep). There are no existing data on which specific rainfall has triggered the landslides. Indeed, the occurrence of landslides in these complexes is not the result of a specific rainstorm event: it rather originates from the combined effects of different events including both extreme short rainfalls, low-intensity long-duration rainfalls, and snow melt. All the landslides mapped in this study are assumed to be shallow translational landslides. Several field surveys were also conducted over the study area in order to map the locations of check dams. Other data, such as detailed channel network information, were provided by the Regional Forestry Service.

## 3. LIDAR DATA SPECIFICATIONS

### 3.1 Rio Cordon basin survey

The LiDAR and photographic data was acquired from an helicopter using an ALTM 3100 OPTTECH, and Rollei H20 Digital camera flying at an average altitude of 1000 m above ground level during snow free conditions in October 2006. The flying speed was 80 knots, the scan angle 20 degrees and the scan rate 71 KHz. The survey design point density was specified to be greater than 5 point per  $\text{m}^2$ , recording up to 4 returns, including first and last.

### 3.2 Miozza basin survey

The LiDAR and photographic data were collected in snow-free conditions during November 2003. The LiDAR and photographic data were acquired from a helicopter flying at an average altitude of 1000 m above ground level and by using an ALTM 3033 OPTECH, and a Rollei H20 Digital camera. The flying speed was 80 knots, the scan angle 20 degrees and the scan rate 33 KHz. The survey design point density was specified to be greater than 2 point per m<sup>2</sup>, recording first and last returns.

## 4. RESULTS AND DISCUSSION

The LiDAR last pulse points were used for the DTMs interpolation at different grid resolutions, which in our case was carried out by applying the ESRI TOPOGRID tool. The TOPOGRID algorithm is a spline technique that uses slope rather than curve information as spline penalty function. This approach has proved (Hutchinson, 1988; Hutchinson, 1989) to limit the occurrence of pits and produce hydrologically correct DTMs, in the sense that there are no pits resulting in internal drainage and incomplete contributing area values.

### 4.1 Analysis of river morphology

High-quality digital terrain data obtained by laser altimetry represent a great improvement in the analysis of surface morphology since a lot of relevant information can be derived from them. Anyway, the use of LiDAR for these types of quantitative analyses is relatively new. In this section we show two examples of the capability of this technology in the detection of the main geometric features of a channel. For the purpose of the analysis firstly we selected the Cordon river (Rio Cordon basin) where the main morphological features were analyzed during past field surveys (Lenzi, 2001) then a channel reach of Miozza basin where some check dams are present. The most common and striking morphological typologies occurring in mountain streams can be categorized as step-pool sequences (Figure 5) (Grant *et al.*, 1990; Billi *et al.* 1998; Lenzi, 1999) and riffle-pool sequences.



Figure 5. An example of step-pool channel reach (courtesy of A. Vianello)

The latter are rarely found when the channel gradient exceeds 3–5 percent (Rosgen, 1994; Montgomery and Buffington, 1997). Step-pool sequences are found within a gradient range between 5 per cent and 30 per cent. Steps are typically formed from accumulations of boulders and cobbles, which span the

channel in a more or less continuous line and separate a backwater pool upstream from a plunge pool downstream. In the Figure 6 is showed the local slope vs. the downstream distance. The patterns of abrupt changing in local slope derived by a 0.5m DTM can be related to the different morphological features of channel reaches.

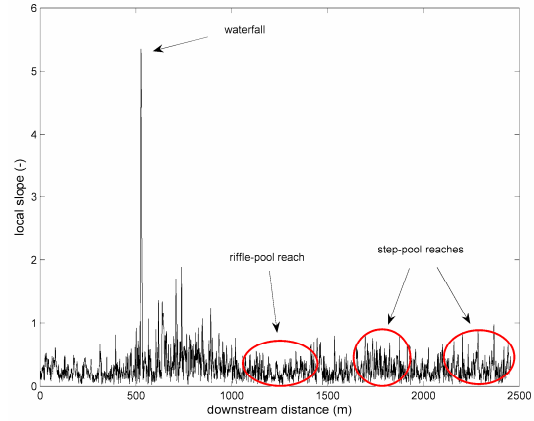


Figure 6. Local slope vs. downstream distance

Low slope reaches are related to riffle-pool morphology units and high slope reaches (especially those sited in proximity of basin outlet) to steep-pool units. Downslope the waterfall (Figure 6) a high slope reach is detected. This part of the river was not accurately investigated in the field but it is believed to be a reach where cascades are present.

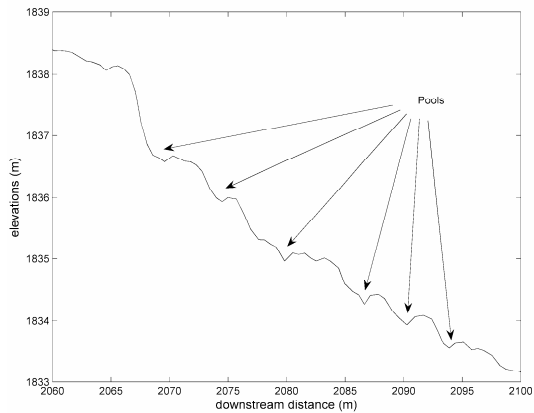


Figure 7. Elevations vs. downstream distance (step-pool reach)

In the Figure 7 and 8 it is showed the elevations profile vs. the downstream distance derived by a 0.5m DTM resolution respectively for a step-pool and riffle-pool reach of Rio Cordon. The pools in the Figure 7 are clearly detected among the steps. The difference of riffle-pool morphology, less step and relatively smooth, is evident in the Figure 8 where the downstream distance and the elevation range are the same of step-pool reach showed in the figure 7. This results suggests a great capability of high resolution LiDAR-derived elevation data in the detection of the main geometric characteristics of step-pool and riffle-pool morphologic units.

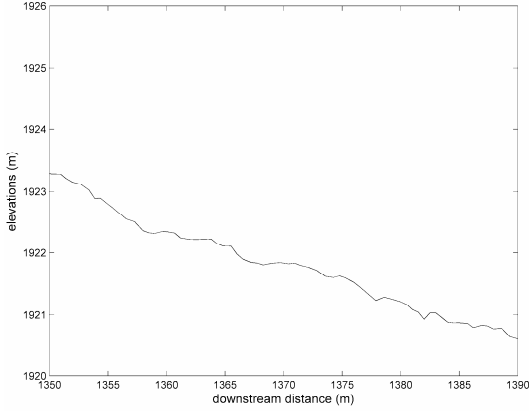


Figure 8. Elevations vs. downstream distance (riffle pool reach)

This approach may be used also in the detection of hydraulic control structure such check dams. In the Figure 9 is showed a reach of the main channel of Miozza basin (Figure 3). We analyzed the local slope channel length derived by a DTM having a grid resolution of 1, 5, 10, and 20m. The numbers indicating the locations of the check dams are also reported (Figure 3).

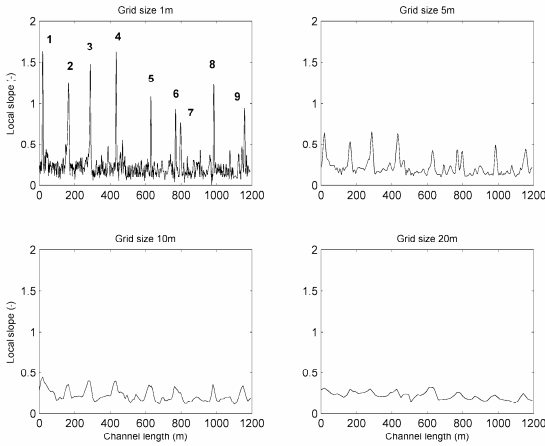


Figure 9. Plots of local slope vs. channel length over different grid sizes. The following numbers reported in the first plot are numbers of check dams reported in Figure 3.

In the first plot, where the slope was derived by a 1m DTM resolution, it is possible to distinguish nine peaks corresponding to the nine check dams numbered in the Figure 3. The higher slope values are associated to the downstream wall of each check dam. Among the peaks, the surface roughness of the river bed is represented by a high density of smaller peaks and small flats. The decreasing resolution of the grid size is reflected in a poorer detection of the surface morphology. In the plots produced with 5m and 10 m grid size, the nine peaks are still marked. However, the bed morphology among the peaks is not so evident as in the first plot. In the fourth plot, a lower resolution (grid cell size of 20m) makes it difficult to locate both the nine peaks and to recognize the surface morphology. Such results suggest that a 1m DTM resolution can provide detailed information on the main morphological features of the terrain surface.

## 4.2 Terrain Stability Modelling

This section reports the scale effect of different DTM resolutions on the potential slope stability mapping. For each of the four digital terrain models which were interpolated with progressively finer grid cell resolutions (20m, 10m, 5m, and 1m), the stability indexes,  $SI$ , from SINMAP (Pack *et al.*, 1998) were used as measures of potential terrain instability. The model applies to shallow translational landsliding phenomena controlled by shallow groundwater flow convergence. It is based upon the infinite slope stability model (e.g. Hammond *et al.*, 1992; Montgomery and Dietrich, 1994) that balances the destabilizing components of gravity and the restoring components of friction and cohesion on a failure plane parallel to the ground surface with negligible edge effects. The safety factor of the infinite slope-stability model (ratio of stabilizing to destabilizing forces) used by SINMAP is given by the following equation

$$FS = \frac{C + \cos \theta \left[ 1 - \min \left( \frac{R}{T} \frac{a}{\sin \theta}, 1 \right) r \right] \tan \phi}{\sin \theta} \quad (1)$$

where  $C$  is the dimensionless cohesion,  $r$  is the ratio of the water density to the soil density ( $\rho_w/\rho_s$ ),  $\theta$  is the slope angle,  $\phi$  is the internal friction angle and  $\min \left( \frac{R}{T} \frac{a}{\sin \theta}, 1 \right)$  is an

estimate of the relative wetness derived on the basis of the TOPMODEL assumptions (Beven and Kirkby, 1979) of steady state drainage driven by a topographic gradient. Dimensionless cohesion,  $C$ , is defined as  $(C_r + C_s)/(h\rho_s g)$ , where  $C_r$  and  $C_s$  are root strength and soil cohesion terms,  $h$  is the thickness of the soil, and  $g$  the gravitational constant. In the expression for the relative wetness,  $a$  (m) is the specific catchment area derived from the DTM (Tarboton, 1997) and  $T$  is the soil transmissivity ( $m^2/hr$ ). In Equation (2),  $a$  and  $\theta$  are derived from the DTM. SINMAP takes the parameters  $C$ ,  $R/T$  and  $\tan \phi$  as uncertain and assumes that each of them has a uniform probability distribution. With respect to these probability distributions, the stability index ( $SI$ ) is defined as the probability that a location is stable, i.e. it has  $FS > 1$  (Pack *et al.*, 1998).

$$SI = \text{prob}(FS > 1) \quad (2)$$

The  $SI$  assumes a range of values varying between 0 and 10, where values closed to 0 indicate areas which are likely to be unstable, and values closed to 10 stand for stable areas.

The addressed question was: what is the influence of high resolution LiDAR-derived DTM on the spatial distribution of the  $SI$  used for the detection of the mapped landslides. The motivation behind this question is shown in Figure 10 (Tarolli and Tarboton, 2005). Due to the surface roughness, when using a fine grid resolution, local slope may not be representative of the reference critical slope in the infinite-slope stability model (Tarolli and Tarboton, 2006). The derived spatial distribution of  $SI$  within a landslide should not be representative for that landslide because both stable and unstable cells are detected for the same landslide area as Figure 10 shows.

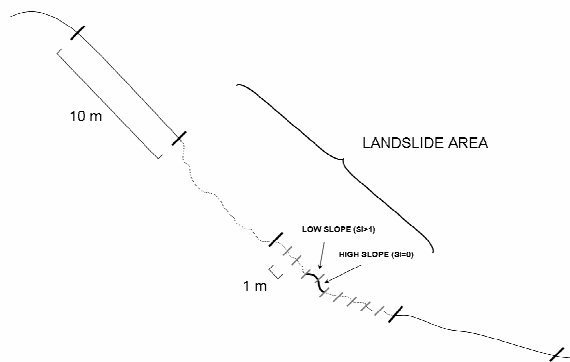


Figure 10. Slope scale effect scheme example about the  $SI$  distribution within a landslide area (Tarolli and Tarboton, 2005).

Calibrated parameters were used to obtain the  $SI$  stability index. We selected four shallow landslides complexes, respectively L1, L2, L3 and L4 in the Figure 3. For each of these, we plotted the  $SI$  along the downslope flow path. This approach was considered for analyzing how surface roughness may affect the spatial distribution of the  $SI$  within a landslide.

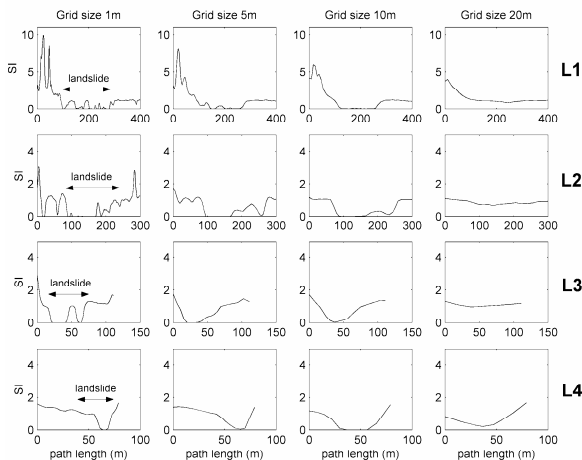


Figure 11.  $SI$  vs. path length plots about field site L1, L2, L3 and L4 over different grid cell sizes.

Figure 11 shows plots of the  $SI$  vs. hillslope length for each analyzed field site. The plots on L1 landslide (first line of plots) show that, with a 1m DTM resolution, the distribution of the  $SI$  within a landslide assumes inconstant values ranging between 0 and 1. This is due to local surface roughness. This result is troublesome because the  $SI$  distribution through a landslide is expected to be 0 or much closed to 0. However, with a 10m DTM resolution the  $SI$  distribution within the landslide assumed values equal to 0. At this resolution it is possible to detect the area of the landslide that places outside it. The results obtained using 20m grid cell size were not acceptable because all the  $SI$  within the landslide assumed values greater than 0.5-1. The plots on landslides L2, L3, and L4 showed similar results. The plot on landslide L3 shows that, with a 1m DTM resolution, the landslide area is interested by a little “flat island” where the  $SI$  values are greater than 1. The landslide is detected with values of  $SI$  equal to 0 by using an intermediate 10m resolution. All

these results suggested that i) the  $SI$  obtained at 1m DTM resolution cannot be representative in the detection of likely unstable areas due to local surface roughness, ii) a 10m DTM resolution overcomes the problem while maintaining a good capability of the  $SI$  in the detection of existing landslides, iii) a 20m DTM resolution is not recommended for these analysis. Anyway these results are sensitive to different topographic roughness elements and thus may be different in some geologic conditions than others (McKean and Roering, 2004).

## 5. FINAL REMARKS

This paper discusses the potential of LiDAR-derived DTM on the analysis of surface morphology, and potential slope stability mapping. The results show a better capability of the DTM grid size less than 5m in the interpretation of the main morphologic features of mountain streams. Otherwise a 10m DTM resolution seems the more appropriate for potential slope stability mapping especially when landslides occur in complexes that where sometimes more than 100m wide. It overcomes the problem of local surface roughness which is perceived at finer grid cell resolutions while maintaining a good capability to depict the topographic characteristics which are relevant for the analysis of terrain stability processes. LiDAR provides high-quality digital terrain data at a resolution higher than previously available; anyway the progressive in finer DTM resolution does not necessarily improve the interpretation of physical processes especially if they occur at a spatial scale greater than grid size. Our results represent only a first look over some applications of LiDAR data in this field. We feel that there is more to be explored to gain new informations on surface morphology and the related physical processes.

## ACKNOWLEDGMENTS

The authors wish to thank the Regional Service of Agricultural, Natural, Forestry and Mountain Resources of the Friuli Venezia Giulia Region and Marco Sangati for their collaboration in the field surveys. The airborne LiDAR and photographic survey of Cordon basin was provided by Helica srl. The research carried out on Miozza basin was supported by the Interreg IIBB Spazioalpino project: CATCHRISK (Mitigation of hydrogeological risk in alpine catchments). The authors are grateful to “Servizio Territorio Montano e Manutenzioni” (Direzione Centrale Risorse Agricole, Naturali, Forestali e Montagna) of Friuli Venezia Giulia Region for the collaboration in field surveys and providing aerial photographs data. LiDAR data of Miozza basin were collected and elaborated within the Interreg IIIA Italy-Slovenia project: “Ricomposizione della cartografia catastale e integrazione della cartografia regionale numerica per i sistemi informativi territoriali degli enti locali mediante sperimentazione di nuove tecniche di rilevamento”.

## REFERENCES

- Ackerman, F., 1999. Airborne laser scanning – present status and future expectations. *IS-PRN Journal of Photogrammetry and Remote Sensing*, 54, pp. 64-67.
- Beven, K.J., Kirkby, M.J., 1979, A physically based variable contributing area model of basin hydrology, *Hydrol. Sci. Bull.*, 24(1), pp. 43–69.
- Billi, P., D’Agostino, V., Lenzi, M.A., Marchi, L., 1998. Bedload, slope and channel processes in a high-altitude alpine torrent. In *Gravel-bed Rivers in the Environment*,

- Klingeman P, Beschta RL, Komar PD, Bradley JB (eds). Water Resources Publications: Colorado, pp.15–38.
- Briese, C., 2004. Breakline Modelling from Airborne Laser Scanner Data. *Ph.D. Thesis*, Institute of Photogrammetry and Remote Sensing, Vienna University of Technology.
- Glenn, N.F., Streutker, D.R., Chadwick, D.J., Tahckray, G.D., Dorsch, S.J., 2006. Analysis of LIDAR-derived topography information for characterizing and differentiating landslide morphology and activity. *Geomorphology*, 73, pp. 131-148.
- Grant, G.E., Swanson, F.J., Wolman, M.G., 1990. Pattern and origin of stepped-bed morphology in high-gradient streams, Western Cascades, Oregon. *Geological Society of America Bulletin*, 102, pp. 340–352.
- Hammond, C., Hall, D., Miller, S., Swetik, P., 1992. Level I Stability Analysis (LISA) Documentation for Version 2.0, General Technical Report INT-285, USDA Forest Service Intermountain Research Station.
- Hutchinson, M.F., 1988. Calculation of hydrologically sound digital elevation models. *Third International Symposium on Spatial Data Handling*, Sydney, Columbus, Ohio: International Geographical Union.
- Hutchinson, M.F., 1989. A new procedure for gridding elevation and stream line data with automatic removal of spurious pits. *Journal of Hydrology*, 106, pp. 211-232.
- Kraus, K., Pfeifer, N., 2001. Advanced DTM generation from LIDAR data. *International Archives of Photogrammetry and Remote Sensing*, XXXIV-3/W4, pp. 23-35.
- Lenzi, M.A., 1999. Morfología y estabilidad de las secuencias en escalones (step-pool) en los torrentes alpinos de elevada pendiente. *Ingeniería del Agua*, 6, pp. 151–162.
- Lenzi, M.A., 2001. Step-pool evolution in the Rio Cordon, Northeastern Italy. *Earth Surface Processes and Landforms*, 26, pp. 991–1008, doi: 10.1002/esp.239.
- Mckean, J., Roering, J., 2004. Objective landslide detection and surface morphology mapping using high-resolution airborne laser altimetry. *Geomorphology*, 57, pp. 331-351, doi:10.1016/S0169-555X(03)00164-8.
- Montgomery, D.R., Dietrich, W.E., 1994. A physically based model for the topographic control on shallow landsliding. *Water Resource Research*, 30(4), pp. 1153-1171.
- Montgomery, D.R., Buffington, J.M., 1997. Channel-reach morphology in mountain drainage basins. *Geological Society of America Bulletin*, 109(5), pp. 596–611.
- Pack, R.T., D.G. Tarboton, and C.N. Goodwin (1998), The SINMAP Approach to Terrain Stability Mapping, 8th Congress of the International Association of Engineering Geology, Vancouver, British Columbia, Canada.
- Rosgen, D.L., 1994. A classification of natural rivers. *Catena*, 22, pp. 169–199.
- Tarboton, D.G., 1997. A new method for the determination of flow directions and upslope areas in grid digital elevation models. *Water Resour. Res.*, 33, pp. 309–319.
- Tarolli, P., Tarboton, D.G., 2005. A New Method for Determination of Most Likely Initiation Points and the Evaluation of Digital Terrain Model Scale in Terrain Stability Mapping. *Eos Trans. AGU*, 86(52): Fall Meet. Suppl., Abstract H51C H51C-0377.
- Tarolli, P., Tarboton, D.G., 2006. A New Method for Determination of Most Likely Landslide Initiation Points and the Evaluation of Digital Terrain Model Scale in Terrain Stability Mapping. *Hydrol. Earth Syst. Sci.*, 10, pp. 663-677.